Nano-Jewels in Biology. Gold and Platinum on Diamond Nanoparticles as Antioxidant Systems Against Cellular Oxidative Stress

Roberto Martín,[†,▽] Cristina Menchón,[‡,▽] Nadezda Apostolova,[§] Victor M. Victor,[§,⊥,∥,#] Mercedes Álvaro,[†] José Raúl Herance,[*,‡] and Hermenegildo García[†,*]

[†]Instituto de Tecnología Química CSIC-UPV and Departamento de Química, Universidad Politécnica de Valencia, Av. De los Naranjos s/n, 46022 Valencia, Spain, [‡]Institut d'Alta Tecnologia-PRBB, c/Dr. Aiguader 88, 08003 Barcelona, Spain, [§]Department of Pharmacology, University of Valencia and CIBERehd, Valencia, Spain, [⊥]University Hospital Doctor Peset Foundation and CIBERehd, Avda Gaspar Aguilar 90, 46017, Valencia, Spain, [∥]University Hospital Doctor Peset, Endocrinology Service, Avda Gaspar Aguilar 90, 46017, Valencia, Spain, and [#]Department of Physiology, University of Valencia, Valencia, Spain. [▽]Co-first authors..

ABSTRACT Diamond nanoparticles (DNPs) obtained by explosive detonation have become commercially available. These commercial DNPs can be treated under Fenton conditions ($FeSO_4$ and H_2O_2 at acidic pH) to obtain purer DNP samples with a small average particle size (4 nm) and a large population of surface OH groups (HO—DNPs). These Fenton-treated HO—DNPs have been used as a support of gold and platinum nanoparticles (≤2 nm average size). The resulting materials (Au/HO—DNP and Pt/HO—DNP) exhibit a high antioxidant activity against reactive oxygen species induced in a hepatoma cell line. In addition to presenting good biocompatibility, Au/HO— and Pt/HO—DNP exhibit about a two-fold higher antioxidant activity than glutathione, one of the reference antioxidant systems. The most active material against cellular oxidative stress was Au/HO—DNP.

KEYWORDS: antioxidant activity of metal nanoparticles · peroxide decomposition by noble metallic nanoparticles · noble metal nanoparticles inside cells · modified diamond nanoparticles as carriers · Fenton treatment of diamond nanoparticles.

Nanoparticles are among the preferred platforms to deliver active molecules and other bioactive species inside living cells.[1−4] Recently, we and others have reported that diamond nanoparticles (DNP) can cross the cell membrane and can be used, among other things, as scaffolds for gen delivery.[5−7] The main advantage of DNPs is their biocompatibility, since the available studies have shown that their presence does not significantly affect the viability of human cervical carcinoma cell lines (HeLa).[7]

DNPs obtained by explosive detonation have become widely available in large quantities and at an affordable price.[8−10] Raw commercial samples contain individual DNP nanoparticles of about 20 nm size that are surrounded and agglomerated by a soot matrix forming large DNP aggregates.[11−14] We have shown that Fenton treatment with hydrogen peroxide is able to remove a large portion of the amorphous carbonaceous residue from commercial samples producing also a reduction of the average DNP size.[12] The Fenton reaction consists of the generation of aggressive hydroxyl radicals (OH·) that are able to promote degradation and partial mineralization of virtually any organic matter.[15−18] In the present case, the Fenton reaction has been used to purify commercial DNPs by the selective mineralization of the soot. The large inertness and robustness of diamonds has been used advantageously to remove the more labile and externally exposed amorphous sp^2 carbons.[19] The harsh conditions of the Fenton reaction are, however, revealed by the side effects of this purification process, such as the surface erosion suffered by DNPs, leading to a particle decrease size and to the formation of a large population of surface OH groups.[12] For this reason the Fenton-treated DNPs will be denoted from now on as HO—DNPs. Considering the DNPs are suitable scaffolds for intracellular delivery and that the presence of OH groups renders the HO—DNP especially suited as a carrier, it occurred to us that supporting noble metal nanoparticles in these materials could combine the ability of DNPs to act as a carrier and the catalytic activity implemented by the presence of the noble metal. In particular, due to the precedents, noble metals could be suitable catalytic sites as antioxidants for dealing with reactive oxygen species (ROS) inside the cells. Therefore, in the present work we describe the biological activity as antioxidant agent

*Address correspondence to hgarcia@qim.upv.es.

Received for review August 6, 2010 and accepted October 07, 2010.

Published online October 12, 2010.
10.1021/nn1019412

© 2010 American Chemical Society

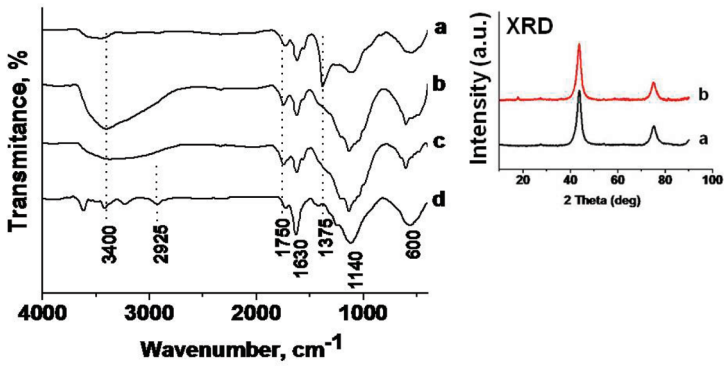

Figure 1. FT-IR spectra of (a) commercial DNP, (b) HO−DNP, (c) Pt/HO−DNP, and (d) Au/HO−DNP. The inset shows the XRD of (a) commercial DNP and (b) Au/HO−DNP.

and the biocompatibility of noble metal nanoparticles supported on Fenton-treated DNP.

We have previously described the catalytic activity of gold for several oxidation reactions and the ability of gold to act as a carbon centered radical quencher.[20,21] Thus, we wanted to evaluate if gold and platinum nanoparticles supported on HO−DNP could be active for intracellular ROS scavenging. The data that will be presented below confirm our hypothesis. We will show that Au/HO−DNP is about two-folds more active to protect human hepatome cell (Hep3B) cells against induced cellular oxidative stress than glutathione, one of the reference compounds with antioxidant properties.[22−27]

RESULTS AND DISCUSSION

One of the most widely used procedures for the preparation of supported metal nanoparticles is the so-called deposition−precipitation method.[28−30] This procedure consists in the anchoring of metal nanoparticle precursors from aqueous solutions onto the surface hydroxyl groups of the support.[28−30] Typically large surface area metal oxides are the solids used as supports for this deposition−precipitation synthesis, but in our case, the large population of hydroxyl groups of HO−DNP makes also this sample suitable for this purpose.

The deposition of gold on HO−DNP [≤2 nm average particle size determined by transmission electron microscopy (TEM)][31] can be followed conveniently by monitoring the OH region of the Fourier transform infrared (FT-IR) spectra of raw DNP, Fenton-treated HO−DNP, and the sample resulting after the deposition of gold (Au/HO−DNP) and platinum (Pt/HO−DNP). Figure 1 presents these spectra showing that, as commented, the Fenton treatment increases considerably the population of OH groups due to the erosion of the DNP surface produced by the attack of •OH radicals to the diamond surface. Anchoring gold on the surface of HO−DNP leads to a considerable decrease in the population of the OH groups, showing that, as expected, they are involved in the deposition of gold and platinum nanoparticles. In addition the Au/HO−DNP sample shows a residual population of isolated (nonhydrogen bonded) hydroxyl groups at about 3650 cm^{-1} and two other small and sharp hydroxyl groups at about 3400 and 3200 cm^{-1}. We noticed also the formation of some CH bonds during the hydrogen treatment to reduce gold.

Besides the HO− region FT-IR spectra of DNPs exhibit some other characteristic bands attributable to esters (1750 cm^{-1}), unsaturated C═C (1630 cm^{-1}), and C−O groups (1140 cm^{-1}). It is interesting to note that these groups are mostly not affected by the Fenton treatment, except the C−O band that increases in intensity. However upon deposition of gold and thermal treatment with hydrogen a significant decrease of the ester vibration peaks is observed. This is again an indication of good interfacial contact between Au and DNP, the former probably acting as catalyst for the hydrogen spill over onto the diamond surface.

The final gold loading on the solid determined by chemical analyses was 0.7%; this is a common gold loading for highly active heterogeneous catalysts.[32,33] The fact that the crystal structure of DNP is preserved after the Fenton treatment was determined by X-ray diffraction (XRD) by comparison of the XRD before and after the Fenton treatment. The low gold loading on Au/HO−DNP precludes however seeing any of the four characteristic diffraction patterns of gold particles (see inset of Figure 1). It is important to assess if gold exhibits a unique activity or if, on the contrary, the antioxidant property is general for most noble metals. In gold catalysis it is always convenient to contrast the activity of gold with that of other noble metals, particularly platinum. For the sake of comparison we prepared

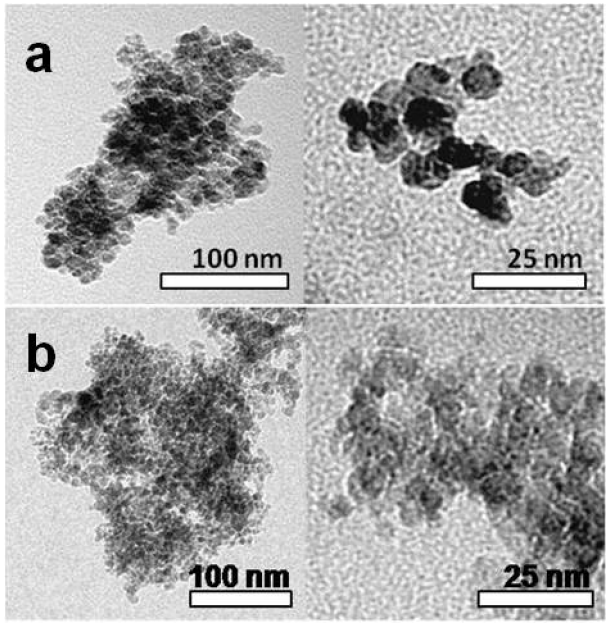

Figure 2. Representative TEM images recorded at two magnifications for (a) Au/HO−DNP and (b) Pt/OH-DNP.

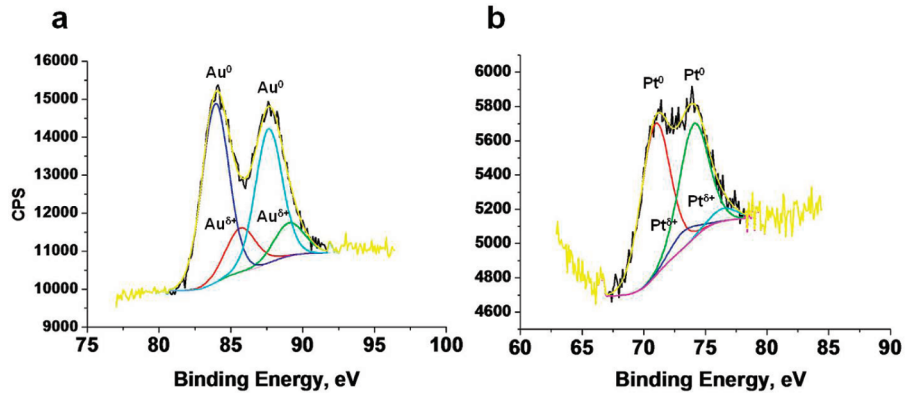

Figure 3. XPS obtained for (a) Au/HO−DNP and (b) Pt/HO−DNP.

analogously a sample of HO−DNP supported platinum nanoparticles (Pt/HO−DNP). The performance of the Pt/HO−DNP sample can serve to delineate the differences in activity and biocompatibility between these two noble metals. The metal loading of Pt/HO−DNP (0.7 wt %) was set to be as close as possible to that of Au/HO−DNP. TEM images of Au/HO−DNP and Pt/HO−DNP show that although there could be a few scattered big nanoparticles larger than 20 nm, the average size of the metal nanoparticles is below to 2 nm, the resolution limit of the electron microscope used. Figure 2 presents representative bright field images of the Au/HO−DNP and Pt/HO−DNP showing that both HO−DNP supported metals contain highly dispersed small nanoparticles.

X-ray photoelectron spectroscopy (XPS) establishes the presence of metal and carbon in Au/HO−DNP and Pt/HO−DNP. Calibration of the intensities of the Au and Pt $4f_{5/2}/4f_{7/2}$ *versus* C 1s gives atomic ratios of 0.042 and 0.043% that are very close to the average values obtained by chemical analyses, assuming that the metals are homogeneously distributed through the sample surface. Deconvolution of the Au $4f_{5/2}$ and $4f_{7/2}$ peaks gives indication of the presence of a small population of positive gold (B.E. 85.7 and 89.1 eV) accompanying the predominant band of the expected Au (0) $4f_{5/2}$ and $4f_{7/2}$ peaks (B.E. 84 and 87.7 eV). Similar treatment of the Pt $4f_{5/2}$ and $4f_{7/2}$ peaks also indicates, as expected, that Pt is almost completely as Pt (0). Figure 3 shows an expansion of the Au and Pt region of XP spectra together with the corresponding deconvolution that allows estimating the relative percentage of the Au and Pt species.

Catalytic Activity to Decompose ROS. As commented previously, our initial hypothesis was that HO−DNP as scaffolds that can cross the cell membrane could be functionalized with noble metal nanoparticles to implement some biocatalytic activity in these otherwise inert DNPs. Gold and platinum were selected as cargos of DNPs because they can trap organic radicals and also exhibit high peroxidase catalytic activity promoting reductive processes and peroxide decomposition.[20,21] We wanted to test the catalytic activity of Au/HO− and Pt/HO−DNP as intracellular antioxidants quenching the ROS, which are responsible for the cellular oxidative stress.

To support this catalytic activity as cellular antioxidant, in preliminary laboratory studies we tested the catalytic activity of Au/HO− and Pt/HO−DNP for the room-temperature decomposition of a diluted aqueous solution of hydrogen peroxide

$$2H_2O_2 \rightarrow 2H_2O + O_2 \qquad (1)$$

The relevance of this catalytic activity in the present case is its potential application in biological systems given that during cellular oxidative stress there is a build up of hydroperoxides which are formed by a reaction of carbon centered radicals with oxygen. Most ROS generating reactions in the cell produce superoxide. However this highly reactive radical is rapidly converted into hydrogen peroxide, a relatively stable molecule. Other organic hydroperoxides are also formed. Therefore, the decomposition of H_2O_2 in solution by these DNP-supported noble metal nanoparticles could be taken as a proof of the activity of Au/HO− and Pt/HO−DNP for the most important intracellular processes coming from oxidative stress.

Figure 4 shows the temporal profile of H_2O_2 decomposition in the presence of Au/HO− and Pt/HO−DNP. As it can be seen there, both materials can decompose

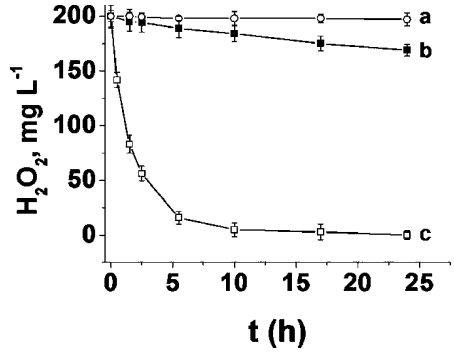

Figure 4. H_2O_2 decomposition activity of HO−DNP supported Au and Pt catalysts for (a) blank in the absence of catalyst, (b) Au/HO−DNP, and (c) Pt/HO−DNP. Reaction conditions: H_2O_2 200 mg L^{-1} (5.88 mM), pH 4, room temperature, and metal 0.0025 mM.

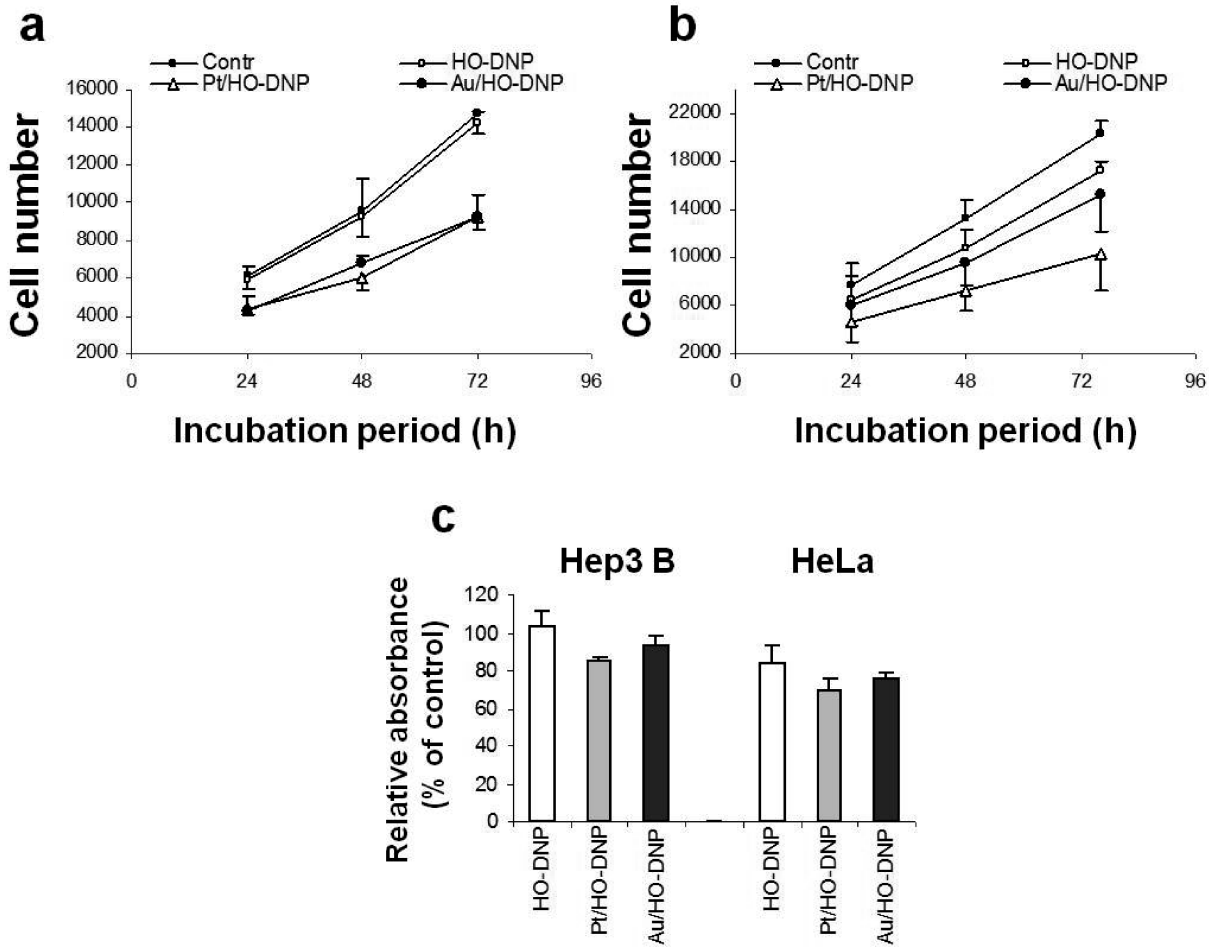

Figure 5. Determination of cellular viability and proliferation. Effect of Pt/HO− and Au/HO−DNP and their carrier HO−DNP on cellular proliferation and viability in (a) Hep3B and (b) HeLa cells. Cell count over 3 days by static cytometry revealed a reduction in cellular proliferation which was visible at 24 h and was maintained over the entire incubation period [data represented as mean ± standard error of the mean (SEM), $n = 3$]. (c) MTT assay of exponentially growing cells after 24 h of culture. Data (mean ± SEM, $n = 5-6$) were analyzed by student's *t* test, significance *versus* control $*p < 0.05$.

diluted solutions of H_2O_2, although the activity of Pt/HO−DNP was about nine times higher than that of Au/HO−DNP. We notice, however, that besides hydrogen peroxide decomposition other parameters, such as radical trapping and biocompatibility, should also be taken into account when evaluating a system as biocatalyst.

As expected in view of the literature precedents, platinum nanoparticles are far more active than gold to decompose H_2O_2 in aqueous solution at room temperature.[31] Nevertheless the profiles given in Figure 4 show that also Au/HO−DNP is active for H_2O_2 decomposition. Typically cellular peroxidases have the role to decompose these hydroperoxides, but under high oxidative stress, this peroxidase activity is not enough to decompose all the hydroperoxides present in the cytosol, and they accumulate producing undesirable side reactions. Thus, the use of antioxidants is necessary in order to maintain the cell redox homeostasis.

Cell Biocompatibility Study Using Au/OH−DNP and Pt/OH−DNP. Due to the promising results obtained of diamond-supported metal nanoparticles as intracellular antioxidants and considering future applications of these materials in biology, we performed a biocompatibility study using common cellular models and assessed the following parameters: (i) cell viability and proliferation and (ii) apoptosis. In order to analyze whether the effect is cell type specific, two cell lines, namely human hepatome cell (Hep3B) and human cervical carcinoma cell line (HeLa) were employed in these studies.

Cellular Viability and Proliferation. Figure 5 shows the effect of Pt/HO− and Au/HO−DNP and their carrier HO−DNP on survival and proliferation of Hep3B and HeLa cells (Figure 5a and b, respectively). Using static cytometry to count cells at 24, 48, and 72 h of incubation, we observed significant differences in the proliferation during the 3 day experimental period with both nanoparticles and in both cell lines. Thus the number of cells counted was lower than in the control at 24 h and remained significantly lower throughout the 72 h period of culture. In both cell lines, the inhibition effect exerted by Pt/OH-DNP was somewhat stronger (particularly for the proliferation of HeLa cells), while the carrier molecule HO−DNP had no significant effect on

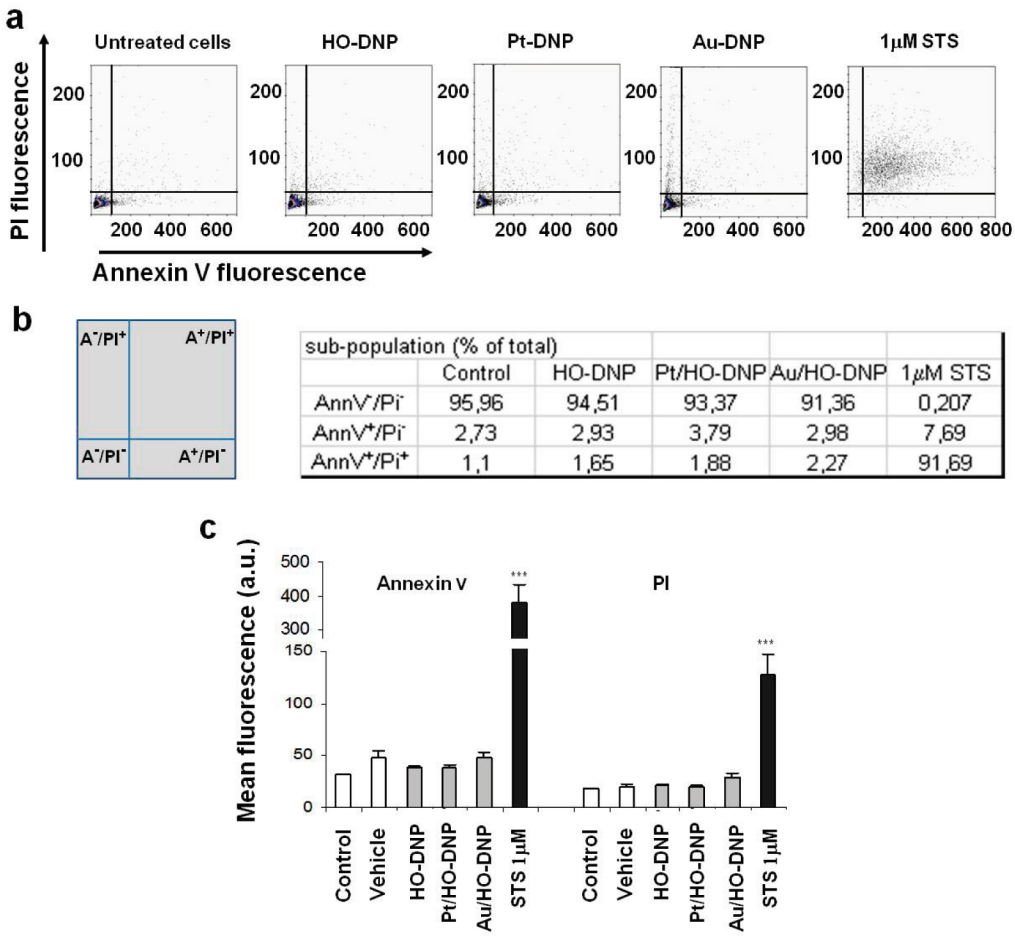

sub-population (% of total)					
	Control	HO-DNP	Pt/HO-DNP	Au/HO-DNP	1μM STS
AnnV⁻/Pi⁻	95,96	94,51	93,37	91,36	0,207
AnnV⁺/Pi⁻	2,73	2,93	3,79	2,98	7,69
AnnV⁺/Pi⁺	1,1	1,65	1,88	2,27	91,69

Figure 6. (a) Representative histograms (Bivariate Annexin V/PI analysis) of untreated control, the carrier HO−DNP, and 1 μM STS-treated cells showing the existence of three cellular subpopulations of the four possible, namely, AnnV⁻/PI⁻, AnnV⁺/PI⁻, and AnnV⁺/PI⁺. (b) Gating diagram showing the different populations for each histogram (four gates). The table shows the % of each subpopulation for all the conditions studied. (c) Summary histogram of AnnexinV and PI fluorescence data. Data (mean ± SEM, $n = 4$) was analyzed by student's *t* test significance *versus* control ***$p < 0.001$.

the cell number. Importantly, none of the antioxidants, not the carrier itself, appeared to affect cellular viability as cells continued proliferating over the evaluated period. The proliferation rate was similar in all treatments and was not significantly different compared to the control (untreated cells).

The MTT assay [colorimetric assay for measuring the activity of enzymes that reduce (3-(4, 5-dimethylthiazol-2-yl)-2,5-diphenyltetrazolium bromide, a yellow tetrazole) to formazan dye, giving a purple color] used to assess cellular viability and proliferation[34] confirmed the static cytometry results of 24 h treatment with the two antioxidants and their carrier. These experiments were also performed in both cell lines. The data obtained are displayed in Figure 5c. In the case of Hep3B cells, only Pt/HO−DNP had a significant effect, the relative absorbance recorded was 85.31 ± 4.77% compared to the control (untreated cells, where the relative absorbance was considered 100%). The absorbance recorded in HeLa cells was statistically different in the case of both Pt/HO−DNP (71.3 ± 5.71% *versus* control) and Au/HO−DNP (69.02 ± 3.91% *versus* control).

Of note, keeping the nanoparticles in the cell culture throughout the entire period of incubation does not exacerbate their effect on the proliferation. Conversely, even a 3 day exposure to the nanoparticles did not induce cytotoxicity. These results were obtained in both the static cytometry and the MTT experiments and in the two cell lines employed.

Apoptosis. In order to confirm and expand the results obtained in the proliferation experiments where we concluded the lack of cytotoxicity, we decided to analyze whether or not the presence of Au/HO− and Pt/HO−DNP triggers the cells apoptosis. These studies were performed in HeLa and Hep3B, and the cells incubated with the nanoparticles for 3 h after which the medium was refreshed and several typical apoptotic parameters were assessed by fluorescence microscopy coupled with static cytometry, at 24 h of treatment (results summarized in Figure 6 for HeLa). The results for Hep 3B where similar than for HeLa (data not shown). The well-known kinase inhibitor staurosporine was employed as a positive pro-apoptotic control. Figure 6c depicts the results of a bivariate Annexin V/PI analysis of exponentially growing HeLa cells. Four different cellu-

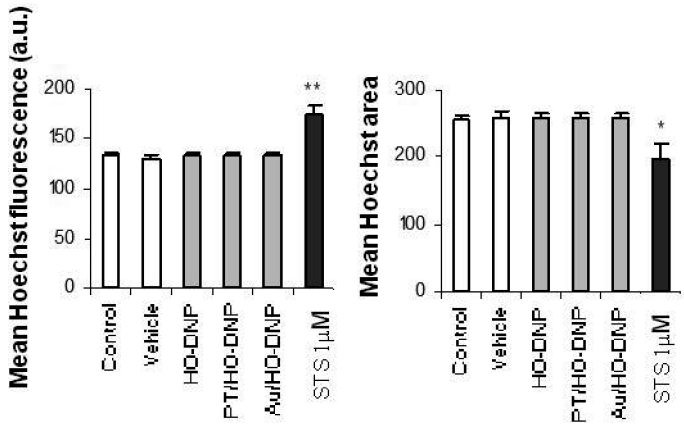

Figure 7. Bar charts representing nuclear morphology changes (mean Hoechst fluorescence and nuclear area); data represented as mean ± SEM, $n = 4$. Statistical analysis was performed by student's t test, $^{*}p < 0.05$ and $^{**}p < 0.01$.

lar subpopulations were evaluated: vital (double negative, Annexin V^-/PI^-), apoptotic (Annexin V^+/PI^-), late apoptotic/necrotic (Annexin V^+/PI^+), and damaged cells (Annexin V^-/PI^+) cells. The cytogram shows a representative experiment in which staurosporine (STS) 1 μM-treated cells displayed apoptotic features, since more than 98% of the cells were apoptotic compared to only 3.7% of the negative control (untreated cells) and 4.5% in the HO−DNP counterpart. Neither of the antioxidant nanoparticles showed a significant increase in the apoptotic cellular subpopulation (cytogram not shown). Figure 6c summarizes the quantification of the mean Annexin V and PI fluorescence.

The typical apoptotic features, chromatin condensation and nuclear fragmentation, were also assessed (Figure 7). For this, the mean intensity of Hoechst fluorescence in each nucleus was quantified as well the area corresponding to this fluorescence. Cells treated with STS 1 μM showed a major increase in mean Hoechst fluorescence (173.75 ± 8.26 *versus* 132.5 ± 2.5 au recorded in the untreated control cells) paralleled by a decrease in the nuclear area (198.75 ± 20.25 *versus* 255 ± 6.77 recorded in the untreated control cells). Again, neither HO−DNP nor the antioxidant nanoparticles exerted any significant effect on these parameters pointing to the absence of chromatin condensation. To conclude, we have not observed any evident apoptosis associated to the exposure of HeLa or Hep3B cells to Pt/HO− or Au/HP−DNP or their carrier HO−DNP.

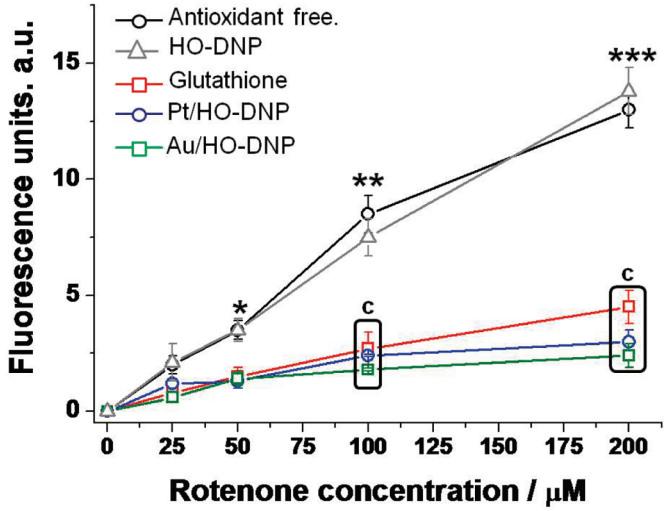

Figure 8. Effect of HO−DNP, glutathione, Pt/HO−DNP, and Au/HO−DNP on rotenone-induced ROS production at different concentrations (25, 50, 100, and 200 μM). The plot shows a DCFH-DA fluorescence decrease in Hep3B cells under different antioxidants. Data represent mean ± SEM ($n = 6$) and were analyzed by student's t test ($^{*}p < 0.05$, $^{**}p < 0.01$, and $^{***}p < 0.001$ *versus* their respective control and "c" surrounded values $p < 0.001$ *versus* their respective treatment group).

Intracellular Activity of Diamond Supported Metal Nanoparticles against Cellular Oxidative Stress. In order to evaluate the antioxidant potential of diamond-supported metal nanoparticles in cells, we chose a commonly used cellular model, Hep3B, and promoted ROS production by the addition of rotenone, a well-known mitochondrial complex I inhibitor,[35−39] in order to increase ROS and to generate analogous cell conditions as those found in the different pathophysiological contexts of oxidative stress. The intracellular level of ROS was determined using a standard procedure, consisting in monitoring intracellular fluorescence of 2,7-dichlorodihydrofluorescein diacetate (DCFH-DA).[40−42] Specific ROS-mediated oxidation of this fluorescent probe leads to the disappearance of its fluorescence. Therefore, loading cells with this fluorochrome and detecting the relative intensity of the emission under different conditions is a common method used to quantify the relative intracellular concentration of ROS.

The antioxidant activity of Au/HO− and Pt/HO−DNP was tested at four different ROS levels generated by the addition of increasing rotenone concentrations (25, 50, 100, and 200 μM) corresponding to different levels of oxidative stress in the cell. The cells were incubated with a complete culture medium containing the diamond-supported metal nanoparticles for 3 h. The fluorescein analogue was added 30 min before washing the cells three times with phosphate buffered saline (PBS). Previous studies have shown that at the concentrations employed in the assays, the presence of DNP does not exert any influence on the viability biocompatibility of cell lines.[7] To put into context the antioxidant activity of the two diamond-supported metal nanoparticles, glutathione and nonmetallic nanodiamond support were also tested, in same concentration of metallic nanoparticles, as controls. The results obtained are shown in Figure 8.

As it can be seen in Figure 8, HO−DNP lacking any noble metal does not exhibit any detectable antioxidant activity. In contrast, a significant reduction of the ROS levels was observed when diamond-supported metal nanoparticles were present in the cell culture. Importantly, the beneficial effect as antioxidant of DNP-supported metal nanoparticles is not linear and be-

comes larger at high ROS concentrations. This phenomenon is certainly positive since high ROS concentrations are most detrimental for the proper cellular function and are a feature observed in many pathologies. These results support the idea that the employed antioxidant systems could be a beneficial tool for the treatment of oxidative stress conditions where there is an elevated production of ROS.

What is important to note is that the data obtained show that, particularly for high ROS concentrations, the catalytic activity as antioxidants of diamond-supported metal nanoparticles is higher than that of glutathione, a typical cellular antioxidant and the most common compound employed as a reference in this type of assay.[22,24,27] Of all the compounds studied, Au/HO−DNP appears to be the most active, probably because it combines peroxidase activity, as presented in Figure 4, and a considerable ability to trap carbon-centered radicals as reported in the literature.[20,21] We propose that this antioxidant stress activity inside cells arises from the combination of DNPs as carriers to cross cells membranes, their ability to graft and stabilize small metal nanoparticles together with the intrinsic antioxidant activity of noble metals promoting the decomposition of ROS. Considering the antioxidant activity and the biocompatibility of Au/HO−DNP, this compound appears as the preferred one over Pt/HO−DNP. However, both nanomaterials have shown a remarkable antioxidant capacity which seems even higher compared to that of glutathione.

CONCLUSIONS

In the present study we have prepared and characterized small gold and platinum nanoparticles supported on Fenton-treated DNPs. These samples exhibit a remarkable biocompatibility without increasing cell mortality and can cross the cellular membrane. These supported noble metal nanoparticles exhibit antioxidant activity decomposing aqueous solutions of hydrogen peroxide. We have presented evidence showing that these diamond-supported metal nanoparticles are powerful antioxidants against the induced cellular oxidative stress. The most promising sample exhibiting higher biocompatibility and peroxidase activity has been the one containing Au.

EXPERIMENTAL SECTION

Fenton Treatment of Commercial Diamond Nanoparticles. Raw diamond nanopowder (1 g) commercially available from Aldrich (ref: 636444, 95+%) was suspended in distilled water (50 mL) in a 500 mL open flask and mixed directly with $FeSO_4 \cdot 7H_2O$ (20 g) as source of Fe^{2+}. After complete dissolution of the ferrous salt, concentrated sulphuric acid (30 mL) was added to the slurry, and the corresponding volume of H_2O_2 (30 wt % in H_2O) (20 mL) was slowly dropped while observing gas evolution. (Caution: The Fenton reaction is highly exothermic and occurs with an evolution of heat and gas. The process must be carried out cautiously in a well-ventilated fume hood wearing goggles and appropriate personal safety items.) This slurry was sonicated on an ice-refrigerated ultrasound bath and held at 1−5 °C for 5 h. Within the first 30 min, the solution turned green/yellow colored, indicative of iron oxidation. After 1 h, additional amounts of H_2SO_4 and H_2O_2 were added, while the suspension becomes yellowish. This second cycle consisting of an addition of reagents and sonication can be repeated a third time, allowing the final cycle to occur for longer times to ensure the complete decomposition of H_2O_2.

After the Fenton treatment, the suspensions were diluted with distilled water and allowed to reach room temperature. The excess of acid was removed performing five consecutive centrifugation−redispersion cycles with Milli-Q water. The diamond nanoparticles were a sediment at the bottom of the centrifuge tube under these conditions. The pH value of the supernatant at the fifth centrifugation−redispersion cycle was neutral. Finally, the Fenton-treated DNPs were submitted to overnight freeze-drying to obtain (HO−DNP) as a brownish dust-like material.

Preparation of Au/HO−DNP and Pt/HO−DNP Catalysts. Au and Pt were deposited on HO−DNP from a solution of $HAuCl_4 \cdot 3H_2O$ (800 mg, 2.35 mmol) or $H_2PtCl_6 \cdot 6H_2O$ (965 mg, 2.35 mmol) in 160 mL of deionized water. The solutions were brought to pH 10 by addition of a 0.1 M aqueous NaOH solution. Once the pH value was stable, the solution was added to a stirred suspension of DNPs in water. After adjusting the pH of the slurry at a value of 10 by addition of a 0.1 M solution of NaOH, the slurry was continuously stirred vigorously for 18 h at room temperature. The resulting Au/HO− or Pt/HO−DNP was collected and dispersed in distilled water. The excess of $HAuCl_4$ and H_2PtCl_6 was removed performing five consecutive centrifugation−redispersion cycles with Milli-Q water. The diamond nanoparticles containing gold were a sediment at the bottom of the centrifuge tube under these conditions. The pH value of the supernatant at the fifth centrifugation−redispersion cycle was neutral, and no traces of chlorides were detected by the $AgNO_3$ test. After removal of the supernatant, the catalysts were dried at vacuum at room temperature for 1 h. Then 150 mg of the supported gold catalysts were placed in a quartz reactor and submitted to reduction under hydrogen atmosphere at 300 °C (heating rate 10 °C min^{-1}) for 6 h. The total Au and Pt contents of the final Au/HO− and Pt/HO−DNP catalyst were 0.7 and 1 wt %, respectively, as determined by chemical analysis. These catalysts are commercially available at argane.diamond@gmail.com.

H_2O_2 Decomposition Test. A series of experiments was carried out in the open air using 200 mg L^{-1} (5.88 mM) of H_2O_2 in the presence of the corresponding catalyst (H_2O_2 to metal molar ratio 2318:1). Prior to the addition of the catalyst, the pH of the solution was set at 4 using 0.01 M HNO_3, and during the H_2O_2 decomposition, the pH was continuously monitored and automatically controlled to pH 4 using a 0.01 M solution of NaOH.

Cell Culture. Experiments were performed with Hep3B (ATCC HB-8064) and HeLa (ATCC CCL-2). Reagents employed in cell culture were purchased from GIBCO (Invitrogen, Eugene, OR). Hep3B cells were cultured in minimum essential medium (MEM) supplemented with 1 mM nonessential amino acids. HeLa cells were cultured in Dulbecco's modification of eagles medium (DMEM) with a high glucose concentration (4.5 mg/mL). Both Hep3B and HeLa culture medias were supplemented with 10% heat-inactivated fetal bovine serum (FBS), penicillin (50 units mL^{-1}), and streptomycin (50 μg mL^{-1}). Cells were maintained in an incubator (IGO 150, Jouan, Saint-Herblain Cedes, France) at 37 °C in a humidified atmosphere of 5% CO_2/95% air (Air-Liquide).

Proliferation and Viability. Cells were seeded in 48-well plates (Falcon, BD) at 20 000 and 10 000 cells/well for Hep3B and HeLa, respectively, and treated with antioxidants or the carrier for 3 h. Then, the medium was refreshed, and the cells were allowed to proliferate exponentially for 3 days. Cells were counted at 24, 48,

and 72 h by static cytometry. For this, 1 μM Hoechst 33342 (nuclear dye) was added in the last 30 min of the treatment, and the cells were then washed with HBSS. All treatments were performed in 4 replicas, and 20 images per well were recorded with a fluorescence microscope (IX81, Olympus, Hamburg, Germany) coupled with a static cytometry software "ScanR" version 2.03.2 (Olympus).

In addition, we performed the MTT (3-[4,5-dimethylthiazol-2-yl]-2,5-diprenyl tetrazolium bromide) assay, which is a colorimetric assay based on the ability of cells to reduce a soluble yellow tetrazolium salt to blue formazan crystals.[43] This reduction takes place only when mitochondrial reductase enzymes are active and is thus a marker of cell viability related to mitochondrial function. For these experiments, cells were seeded in 96-well plates (Falcon, BD) at 20 000 and 10 000 cells/well for Hep3B and HeLa, respectively. Treatment was performed over 3 h, then the medium was refreshed, and the cells were further cultured for a total of a 24 h period. MTT reagent (Roche Diagnostics, Mannheim, Germany) was added (20 μL/well) for the last 4 h of the treatment. Cells were solubilized with dimethyl sulfoxide (DMSO) (100 μL/well, 5 min, 37 °C), and absorbance was measured using a "Multiscan" plate-reader spectrophotometer (Thermo Labsystems, Thermoscientific, Rockford, IL). Results were obtained subtracting the absorbance at 690 nm background absorbance from the 570 nm absorbance, as indicated in the instructions provided with the kit.

Apoptosis. Induction of apoptosis was studied by Bivariate Annexin V/PI analysis for which HeLa and Hep3B cells were used in duplicate in 48-well plates. Treatment was performed over 3 h, then the medium was refreshed, and the cells were further cultured for a total of 24 h period. Then, the medium was replaced with HBSS containing 1 μM of the chromatin-specific dye Hoechst 33342 and 1 μL Annexin V-fluorescein in order to detect phosphatidyl serine exteriorization and was incubated in the dark for 15 min at 37 °C. Thereafter, 0.5 μL of the chromatin-detecting dye propidium iodide (PI) was added (5 min) to label dead or damaged cells. Annexin V and PI solutions were purchased in the form of Annexin-V-FLUOS staining kit (Roche Diagnostics, Mannheim, Germany). Staurosporine (STS), a widely used protein kinase inhibitor, was employed as a positive proapoptotic control.[44] Analysis was performed in 16−30 images per well and was recorded with a fluorescence microscope (IX81, Olympus, Hamburg, Germany) coupled with a static cytometry software "ScanR" version 2.03.2 (Olympus).

ROS Production. ROS production was analyzed in cells seeded in a black 96-well plate.[45] Cells were treated with antioxidants, the carrier (20 μg/mL), or GSH (100 μM) for 3 h. The fluorescent probe DCFH-DA (2′,7′-dichlorodihydrofluorescein diacetate, 2.5 μM) was added in the last 30 min of incubation. After that, cells were washed with PBS three times, and fluorescence was detected at 5 min intervals over a 30 min period using a Fluoroskan (Thermo Labsystems, Thermo Scientific, Rockford, IL). High concentrations of rotenone (25, 50, 100, and 200 μM) were used as a positive control.

Acknowledgment. This study was financed by grants CTQ2007-67805-AR07, CTQ2009-11567, ACOMP 2010/169, and CIBERehd. V.M.V. is the recipient of a Fondo de Investigacion Sanitaria (FIS) contract (CP07/00171). R.M. also thanks the Spanish Ministry of Education for a postgraduate scholarship.

REFERENCES AND NOTES

1. Akerman, M. E.; Chan, W. C. W.; Laakkonen, P.; Bhatia, S. N.; Ruoslahti, E. Nanocrystal Targeting in Vivo. *Proc Natl Acad Sci U.S.A.* **2002**, *99*, 12617–12621.
2. Gao, X. H; Cui, Y. Y; Levenson, R. M; Chung, L. W. K; Nie, S. M. In Vivo Cancer Targeting and Imaging with Semiconductor Quantum Dots. *Nat. Biotechnol.* **2004**, *22*, 969–976.
3. Ito, A; Shinkai, M; Honda, H; Kobayashi, T. Medical Application of Functionalized Magnetic Nanoparticles. *J. Biosci. Bioeng.* **2005**, *100*, 1–11.
4. Mao, H.-Q.; Roy, K.; Troung-Le, V. L.; Janes, K. A.; Lin, K. Y.; Wang, Y.; August, J. T.; Leong, K. W. Chitosan-DNA Nanoparticles as Gene Carriers: Synthesis, Characterization and Transfection Efficiency. *J. Controlled Release* **2001**, *70*, 399–421.
5. Faklaris, O.; Garrot, D.; Joshi, V.; Druon, F.; Boudou, J. P.; Sauvage, T.; Georges, P.; Curmi, P. A.; Treussart, F. Detection of Single Photoluminescent Diamond Nanoparticles in Cells and Study of the Internalization Pathway. *Small* **2008**, *4*, 2236–2239.
6. Faklaris, O.; Joshi, V.; Irinopoulou, T.; Tauc, P.; Sennour, M.; Girard, H.; Gesset, C.; Arnault, J.-C.; Thorel, A.; Boudou, J.-P.; Curmi, P. A.; Treussart, F. Photoluminescent Diamond Nanoparticles for Cell Labeling: Study of the Uptake Mechanism in Mammalian Cells. *ACS Nano* **2009**, *3*, 3955–3962.
7. Martin, R.; Alvaro, M.; Herance, J.-R.; Garcia, H. Fenton-Treated Functionalized Diamond Nanoparticles as Gene Delivery System. *ACS Nano* **2010**, *4*, 65–74.
8. Krueger, A. Diamond Nanoparticles: Jewels for Chemistry and Physics. *Adv. Mater.* **2008**, *20*, 2445–2449.
9. Krueger, A. New Carbon Materials: Biological Applications of Functionalized Nanodiamond Materials. *Chem.—Eur. J.* **2008**, *14*, 1382–1390.
10. Chukhaeva, S. I. Synthesis, Properties, And Applications of Fractionated Nanodiamonds. *Phys. Solid State* **2004**, *46*, 625–628.
11. Krueger, A.; Boedeker, T. Deagglomeration and Functionalization of Detonation Nanodiamond with Long Alkyl Chains. *Diamond Relat. Mater.* **2008**, *17*, 1367–1370.
12. Martin, R.; Heydorn, P.-C.; Alvaro, M.; Garcia, H. General Strategy for High-Density Covalent Functionalization of Diamond Nanoparticles Using Fenton Chemistry. *Chem. Mater.* **2009**, *21*, 4505–4514.
13. Krueger, A.; Liang, Y.; Jarre, G.; Stegk, J. Surface Functionalization of Detonation Diamond Suitable for Biological Applications. *J. Mater. Chem.* **2006**, *16*, 2322–2328.
14. Spitsyn, B. V.; Gradoboev, M. N.; Galushko, T. B.; Karpukhina, T. A.; Serebryakova, N. V.; Kulakova, I. I.; Melnik, N. N. Purification and Functionalization of Nanodiamond. *NATO Sci. Ser., II* **2005**, *192*, 241–252.
15. Fenton, H. J. H. Oxidation of Tartaric Acid in Presence of Iron. *J. Chem. Soc., Trans.* **1894**, *65*, 899–911.
16. Haber, F.; Weiss, J. The Catalysis of Hydrogen Peroxide. *Naturwissenschaften* **1932**, *20*, 948–950.
17. Haber, F.; Weiss, J. *Proc. R. Soc. London* **1934**, *147*, 332–351.
18. Buxton, G. V.; Greenstock, C.l. Critical Review of Rate Constants for Reactions of Hydrated Electrons, Hydrogen Atoms and Hydroxyl Radicals (· OH/ · O-) In Aqueous Solution. *J. Phys. Chem.* **1988**, *17*, 513–886.
19. Barnard, A. S. Stability of Nanodiamond. *Ultrananocryst. Diamond* **2006**, 117–154.
20. Alvaro, M.; Aprile, C.; Corma, A.; Ferrer, B.; Garcia, H. Influence of Radical Initiators in Gold Catalysis: Evidence Supporting Trapping of Radicals Derived from Azobis(Isobutyronitrile) By Gold Halides. *J. Catal.* **2007**, *245*, 249–252.
21. Aprile, C.; Boronat, M.; Ferrer, B.; Corma, A.; Garcia, H. Radical Trapping by Gold Chlorides Forming Organogold Intermediates. *J. Am. Chem. Soc.* **2006**, *128*, 8388–8389.
22. Hayes, J. D.; Flanagan, J. U.; Jowsey, I. R. Glutathione Transferases. *Annu. Rev. Pharmacol. Toxicol.* **2005**, *45*, 51–88.
23. Hayes, J. D.; McLellan, L. I. Glutathione and Glutathione-dependent Enzymes Represent a Co-ordinately Regulated Defence against Oxidative Stress. *Free Radical Res.* **1999**, *31*, 273–300.
24. Meister, A. Glutathione-ascorbic Acid Antioxidant System in Animals. *J. Biol. Chem.* **1994**, *269*, 9397–9400.
25. Rushmore, T. H.; Morton, M. R.; Pickett, C. B. The Antioxidant Responsive Element. Activation by Oxidative Stress and Identification of the DNA Consensus Sequence Required for Functional Activity. *J. Biol. Chem.* **1991**, *266*, 11632–11639.
26. Valko, M.; Rhodes, C. J.; Moncol, J.; Izakovic, M.; Mazur, M. Free Radicals, Metals and Antioxidants in Oxidative Stress-induced Cancer. *Chem.-Biol. Interact.* **2006**, *160*, 1–40.

27. Wu, G. Y.; Fang, Y. Z.; Yang, S.; Lupton, J. R.; Turner, N. D. Glutathione Metabolism and Its Implications for Health. *J. Nutr.* **2004**, *134*, 489–492.
28. Bamwenda, G. R.; Tsubota, S.; Nakamura, T.; Haruta, M. The Influence of the Preparation Methods on the Catalytic Activity of Platinum and Gold Supported on TiO_2 for CO Oxidation. *Catal. Lett.* **1997**, *44*, 83–87.
29. Haruta, M. Size- and Support-Dependency in the Catalysis of Gold. *Catal. Today* **1997**, *36*, 153–166.
30. Tsubota, S.; Cunningham, D. A. H.; Y. Bando, Y.; Haruta, M. Preparation of Nanometer Gold Strongly Interacted with TiO2 and the Structure Sensitivity in Low-temperature Oxidation of CO. *Stud. Surf. Sci. Catal.* **1995**, *91*, 227–235.
31. Navalon, S.; Martin, R. M. ; Alvaro, M. ; Garcia, H. *Angew. Chem., Int. Ed.* **2010**, DOI: 10.1002/anie.201003216.
32. Corma, A.; Garcia, H. Supported Gold Nanoparticles as Catalysts for Organic Reactions. *Chem. Soc. Revs.* **2008**, *37*, 2096–2126.
33. *Supported Gold Nanoparticles as Oxidation Catalysts*; Corma, A.; Garcia, H. Eds.; Wiley & Sons: Weinheim, Germany, 2008.
34. Mossmann, T. *J. Inmunol. Meth.* **1983**, *65*, 55–63.
35. Dugan, L. L.; Sensi, S. L.; Canzoniero, L. M. T.; Handran, S. D.; Rothman, S. M.; Lin, T. S.; Goldberg, M. P.; Choi, D. W. Mitochondrial Production of Reactive Oxygen Species in Cortical Neurons following Exposure to N-methyl-D-aspartate. *J. Neurosci.* **1995**, *15*, 6377–6388.
36. Garciaruiz, C.; Colell, A.; Morales, A.; Kaplowitz, N.; Fernandezcheca, J. C. Role of Oxidative Stress Generated from the Mitochondrial Electron Transport Chain and Mitochondrial Glutathione Status in Loss of Mitochondrial Function and Activation of Transcription Factor Nuclear Factor-κB: Studies with Isolated Mitochondria and Rat Hepatocytes. *Mol. Pharmacol.* **1995**, *48*, 825–834.
37. QuilletMary, A.; Jaffrezou, J. P.; Mansat, V.; Bordier, C.; Naval, J.; Laurent, G. Implication of Mitochondrial Hydrogen Peroxide Generation in Ceramide-induced Apoptosis. *J. Biol. Chem.* **1997**, *272*, 21388–21395.
38. Sherer, T. B.; Betarbet, R; Testa, C. M.; Seo, B. B.; Richardson, J. R.; Kim, J. H.; Miller, G. W.; Yagi, T; Matsuno-yagi, A; Greenamyre, T. Mechanism of Toxicity in Rotenone Models of Parkinson's Disease. *J. Neurosci.* **2003**, *23*, 10756–10764.
39. Sherer, T. B.; Kim, J. H.; Betarbet, R.; Greenamyre, J. T. Subcutaneous Rotenone Exposure Causes Highly Selective Dopaminergic Degeneration and α-synuclein Aggregation. *Exp. Neurol.* **2003**, *179*, 9–16.
40. Afri, M.; Frimer, A. A.; Cohen, Y. Active Oxygen Chemistry within the Liposomal Bilayer Part IV: Locating 2′,7′-dichlorofluorescein (DCF), 2′,7′-dichlorodihydrofluorescein (DCFH) And 2′,7′-dichlorodihydrofluorescein Diacetate (DCFH-DA) In the Lipid Bilayer. *Chem. Phys. Lipids.* **2004**, *131*, 123–133.
41. Brubacher, J. L.; Bols, N. C. Chemically De-acetylated 2′,7′-dichlorodihydrofluorescein Diacetate as a Probe of Respiratory Burst Activity in Mononuclear Phagocytes. *J. Immunol. Methods.* **2001**, *251*, 81–91.
42. Yang, H. W.; Hwang, K. J.; Kwon, H. C.; Kim, H. S.; Choi, K. W.; Oh, K. S. Detection of Reactive Oxygen Species (ROS) And Apoptosis in Human Fragmented Embryos. *Hum. Reprod.* **1998**, *13*, 998–1002.
43. Mosmann, T. *J. Immunol. Methods* **1983**, *65*, 55–63.
44. Lakhani, S. A.; Masud, A.; Kuida, K.; Porter, G. A. J.; Booth, C. J.; Mehal, W. Z. Caspases 3 and 7: Key Mediators of Mitochondrial Events of Apoptosis. *Science* **2006**, *311*, 847–851.
45. Esplugues, J. V.; Rocha, M.; Nuñez, C.; I.; Boscá, I.; Ibiza, S.; Herance, J.-R. Complex I Dysfunction and Tolerance to Nitroglycerin: An Approach Based on Mitochondrial-targeted Antioxidants. *Circ. Res.* **2006**, *99*, 1067–1075.